Manuscript Details

Manuscript number	DSR2_2018_151
Title	Zr/Hf RATIO AND REE BEHAVIOUR: A COUPLED INDICATION OF TERRESTRIAL INPUT IN MARGINAL BASINS AND DEEP-SEA BRINES
Article type	Full length article

Abstract

The distribution of the dissolved Zr and Hf concentrations in the Eastern Mediterranean seawater column was measured in the Kryos basin to evaluate the contribution of the delivery of lithogenic materials from the continent represented by the atmospheric dust from Sahara and Arabian deserts and by the concurrent input from the Nile river. We found that in shallow waters the Zr/Hf ratio shows sub-chondritic values corresponding to the dissolution of Hf enriched products, represented by Mn-rich varnish coating desert particles. In deeper waters, the Z/Hf recorded value is mainly chondritic or slight higher corresponding to the different Zr and Hf aqueous-complex stability and surface reactivity onto surfaces of authigenic suspended particles. The Zr/Hf value of the lower seawater column up to 3300m corresponds to the value found in the Atlantic Ocean. The REE distribution in the Kryos seawater displayers a negative Ce anomaly and a positive La anomaly along the shallow waters above 75 m depth while they do not appear in the seawater below 75 m. Further analyses of Zr, Hf and REE concentration measured in the anoxic deep-sea brines from Tyro, Medee and Thetis basins indicate that the dissolution of evaporite Messinian levels are responsible of the high salt contents of these brines and influence the Zr-Hf fractionation in aqueous phase. The larger affinity of Hf towards surfaces of several sedimentary minerals as salts and Fe-oxyhydroxides relative to Zr and the observed shale-normalised REE features suggest that the leaching of Zr, Hf and REE from Fe-rich coatings of desert particles in shallow seawater and from Messinian evaporites in deep-sea brine can be responsible of the observed distribution of Zr/Hf values and REE behaviour in studied Eastern Mediterranean seawater.

Corresponding Author	Paolo Censi
Order of Authors	Paolo Censi, Maria Raso, Filippo Saiano, Pierpaolo Zuddas, Elvira Oliveri

Submission Files Included in this PDF

File Name [File Type]

Cover letter.doc [Cover Letter]

Manuscript.docx [Manuscript File]

Fig. 1.pdf [Figure]

Fig. 2.pdf [Figure]

Fig. 3.pdf [Figure]

Fig. 4.pdf [Figure]

Fig. 5.pdf [Figure]

Fig. 6.pdf [Figure]

Fig. 7.pdf [Figure]

To view all the submission files, including those not included in the PDF, click on the manuscript title on your EVISE Homepage, then click 'Download zip file'.

Research Data Related to this Submission

There are no linked research data sets for this submission. The following reason is given:
Data will be made available on request

Paolo Censi
Dipartimento DISTEM
University of Palermo
Via Archirafi, 36
90123 Palermo
(ITALY)

Palermo, November 14th, 2018

Dear Sir,

please, find enclosed a copy of the manuscript “Zr/Hf RATIO AND REE BEHAVIOUR: A COUPLED INDICATION OF TERRESTRIAL INPUT IN MARGINAL BASINS AND DEEP-SEA BRINES” that has been just submitted to *Deep-Sea Research II* hoping that it can be enclosed in the Eastern Mediterranean special issue.

In our manuscript we report original results about REE, Zr and Hf distributions in the eastern Mediterranean. Our data show the impact of the delivery of airborne particles on the composition of the shallowest water column in the Kryos basin. The extent of this effect can be assessed according to the evolution of Zr/Hf ratio and the features of shale-normalised REE patterns along the water column. At the same time, our research also focuses how the change of Zr/Hf ratio and the REE distribution can be influenced through the dissolution of evaporite sediments responsible of Eastern Mediterranean deep-sea brines in Thetis, Medee and Tyro basins. Therefore, taking in account the novelty of this paper in terms of geochemical approach, we hope that this can be positively considered for the publication on *the* Eastern Mediterranean special issue *of Deep-Sea Research II*.

Sincerely yours,
Paolo Censi

Zr/Hf RATIO AND REE BEHAVIOUR: A COUPLED INDICATION OF TERRESTRIAL INPUT IN MARGINAL BASINS AND DEEP-SEA BRINES

Censi P.[1*], Raso M.[1], Saiano F.[2], Zuddas P.[3], Oliveri E.[4]

1. D.I.S.T.E.M. department, University of Palermo, Via Archirafi, 22 90123 Palermo, Italy
2. S.A.F. department, University of Palermo, Viale delle Scienze 4, 90128 Palermo, Italy
3. Sorbonne Université, Metis, 4, place Jussieu F75005 Paris, France
4. IAMC-CNR, UOS Capo Granitola, via del Mare, 3, 91021 Campobello di Mazara, Italy

* Corresponding author: paolo.censi@unipa.it

Abstract

The distribution of the dissolved Zr and Hf concentrations in the Eastern Mediterranean seawater column was measured in the Kryos basin to evaluate the contribution of the delivery of lithogenic materials from the continent represented by the atmospheric dust from Sahara and Arabian deserts and by the concurrent input from the Nile river.

We found that in shallow waters the Zr/Hf ratio shows sub-chondritic values corresponding to the dissolution of Hf enriched products, represented by Mn-rich varnish coating desert particles. In deeper waters, the Z/Hf recorded value is mainly chondritic or slight higher corresponding to the different Zr and Hf aqueous-complex stability and surface reactivity onto surfaces of authigenic suspended particles. The Zr/Hf value of the lower seawater column up to 3300m corresponds to the value found in the Atlantic Ocean.

The REE distribution in the Kryos seawater displayers a negative Ce anomaly and a positive La anomaly along the shallow waters above 75 m depth while they do not appear in the seawater below 75 m. Further analyses of Zr, Hf and REE concentration measured in the anoxic deep-sea brines from Tyro, Medee and Thetis basins indicate that the dissolution of evaporite Messinian levels

are responsible of the high salt contents of these brines and influence the Zr-Hf fractionation in aqueous phase.

The larger affinity of Hf towards surfaces of several sedimentary minerals as salts and Fe-oxyhydroxides relative to Zr and the observed shale-normalised REE features suggest that the leaching of Zr, Hf and REE from Fe-rich coatings of desert particles in shallow seawater and from Messinian evaporites in deep-sea brine can be responsible of the observed distribution of Zr/Hf values and REE behaviour in studied Eastern Mediterranean seawater.

1. INTRODUCTION

The distribution of the Zr/Hf values in seawater has been right now investigated by about twenty studies focused on methodology (Firdaus et al., 2007; 2018; Raso et al., 2013), on the composition of estuaries and coastal waters (McKelvey and Orians, 1998; Godfrey et al., 1996; 2008; 2009; Rickli et al., 2014; Firdaus et al., 2015; Censi et al., 2018) and on the distribution of Zr/Hf in open ocean water (Firdaus et al., 2011). Recently, Firdaus et al. (2018) studied seawater samples from Atlantic, Indian Oceans and coastal areas from the Thailand Gulf and Andaman sea. Obtained results suggest that the aqueous Zr-Hf fractionation can be significantly influences by coastal input of terrestrial solids.

At the same time, several researches investigated the different Zr and Hf behaviour at the dissolved pool - Mn-, Fe-oxyhydroxides interface (Koschinsky and Hein, 2003; 2017; Bau and Koschinsky, 2009; Hein et al., 2013; Schmidt et al., 2014; Hein and Koschinsky, 2014) since these are among the most significant authigenic marine sediments and a potential source of REE and other trace elements.

Mn-, Fe-oxyhydroxides are an important component of the atmospheric dust and it is considered a significant source of trace elements for seawater also in open ocean (Tachikawa et al., 1997; 1999; Greaves et al., 1999; Guieu, 1999; Guieu et al., 2018; Louis et al., 2018; Richon et al.,

2018 and references therein). But the impact of the dissolution of atmospheric dust on the distribution of Zr, Hf and REE in seawater is poorly studied.

In order to address such lack of knowledge, this study was carried out focusing its interest on the water column of Kryos basin in the Eastern Mediterranean Sea where the Sahara and Arabian deserts represent a good source of atmospheric dust particles rich in Mn-, Fe-oxyhydroxides. Moreover, the Eastern Mediterranean Sea is probably one of the best examples of a marginal basin where the effect of riverine input from Nile, one of the largest rivers worldwide, can be studied. Moreover, REE distribution in Mediterranean was mainly studied in Western and Central basins (Greaves et al., 1991; 1994; Censi et al., 2004; 2007; 2010) rather than in the Eastern area (Schijf et al., 1995; Bau et al., 1997). Moreover, in the Eastern Mediterranean basin sometimes the oxic water column lies over depressed seafloor areas filled by the accumulation of brines coming from the dissolution of Messinian evaporites (Cita, 2006 and references therein). This process is a further example of a lithogenic contribution likely to influence the geochemical behaviour of dissolved Zr, Hf and REE in seawater that deserves further attention in order to improve the knowledge of the geochemical behaviour of these elements in Eastern Mediterranean.

2. MATERIALS AND METHODS

In the Eastern Mediterranean basin two submerged mountain chains ranging from Ionian Sea to Levantine Basin occur. While crests reach about 1500 m below the sea surface, abyssal plans are located between 3500 and 4000 m depth (Camerlenghi, 1990). The alternating occurrence of basins and ridges allowed to a particular seafloor topography probably induced by presence of Messinian evaporites lying immediately below thin hemipelagic sediments (Ryan et al., 1973; Hsu et al., 1978). In some depressions of this topography deep lakes filled by hypersaline brines were discovered from 1983 below natural oxygenated seawater (Camerlenghi, 1990 and references therein) and others undiscovered brine lakes probably also occur in the same area (Medriff Consortium, 1995). In this context, during the oceanic cruise MAMBA 2010, carried out with RV Urania, other anoxic brines

78 were investigated in the Bannock (collection point Thetis and Medea) and Tyro basins. Collections
79 of oxic seawater samples were carried out in the Bannock basin where a whole deep oxic water
80 column was collected in the Kryos area and a seawater samples immediately up the oxic-anoxic
81 interface was collected in the Thetis basin. Locations of investigated areas are reported in Figure 1.
82 The sampling system of seawater samples consisted of a Neil-Brown CTD rosette frame and
83 24x12 l Teflon-lined GoFlo bottles. Upon recovery of the GoFlo bottles, water samples were
84 immediately filtered through 0.45 μm Millipore® filters in order to reduce further dissolution of the
85 labile particulate fraction, using a Teflon filtering manifold, and acidified to pH 1-2 with HNO_3
86 (Baker Ultrex II®). All the water samples were processed in a laminar flow clean bench to minimise
87 contamination and all sampling materials were previously cleaned with high purity grade reagents
88 (Baker Ultrex II®). All the materials used to collect and manipulate water samples were plasticware
89 and were acid cleaned with 1:10 hot high purity HNO_3 solutions.
90 Therefore, collected seawater samples (4 litres) were added with Fe standard solution and pH
91 was adjusted to 8.0 using concentrated ammonium hydroxide solution. To allow the homogenization
92 and the precipitation of Fe-hydroxide, the treated sample was continuously stirred for two hours and
93 left to mature for two days. Then, the obtained precipitate was filtered and the Fe-hydroxide removed
94 by filtration, washed with ultra-pure water, and subsequently dissolved in HCl 6 mmol ml^{-1}. After a
95 further dilution in high purity grade water ($\rho \geq 18.2$ MΩ) the sample solution was analysed in Q-ICP-
96 MS (Agilent 7500). All used products were high purity grade chemicals (Baker chemicals). Extensive
97 chemometric investigations on the used methods and related uncertainly are reported in Raso et al.
98 (2013).
99 The above-mentioned method allowed to obtain simultaneous determinations of REE, Zr and
100 Hf from the same seawater aliquot coprecipitating requested elements onto freshly-formed $Fe(OH)_3$.
101 Therefore, the new methodology was pointed out and extensively described in Raso et al. (2013).
102 This method exploits the affinity of all the studied elements as regards of the coprecipitation in
103 presence of $Fe(OH)_3$ in order to separate REE, Zr and Hf from the highly saline seawater matrix

104 enriching them onto a freshly-formed $Fe(OH)_3$ solid. Therefore, the co-precipitation of these elements
105 onto $Fe(OH)_3$ was carried out in presence of an excess of ammonium ions avoiding the precipitation
106 of Zn^{2+}, Ni^{2+}, Cu^{2+} and Co^{2+}, due to the formation of complexes with ammonia $[Co(NH_3)_4]^{2+}$,
107 $[Ni(NH_3)_6]^{2+}$, $[Zn(NH_3)_4]^{2+}$, as well as precipitation of alkaline earth metal.

108 The shale normalised REE concentration was assessed with respect to Post Archean Australian
109 Shale (PAAS; Taylor and McLennan, 1995) by the equation:

110 $$[REE]_{sn} = \frac{[REE]_{sa}}{[REE]_{PAAS}} \quad (1)$$

111 where $[REE]_{sa}$ is the concentration of each rare earth measured in the analysed samples and
112 $[REE]_{PAAS}$ is the concentration of the same element measured in PAAS. The extent of Ce depletion
113 (or accumulation) recognised from the normalised concentrations are defined in terms of "anomaly"
114 as follows:

115 $$\frac{Ce}{Ce^*} = \frac{2 \times [Ce]_{sn}}{[La]_{sn} + [Pr]_{sn}} \quad (2)$$

116 (Alibo and Nozaki, 1999). For Gd, the anomaly assessment is carried out according to the equation:

117 $$\frac{Gd}{Gd^*} = \frac{\sqrt{[Ho]_{sn}} \times [Gd]_{sn}}{\sqrt[3]{Tb_{sn}^2}} \quad (3)$$

118 (Moller et al., 2007). In both equations the "sn" suffix indicates shale-normalised concentrations.
119
120 ## 3. RESULTS
121 ### *3.1 Oxic waters*
122 These analyses correspond to the seawater column in Kryos basin from 25 to 3238 m depth.
123 Moreover, a sample from the deep seawater column was collected in Thesis basin at 3305 m depth.
124 The composition of studied elements in water samples are reported in Tab. 1.
125 Zirconium and Hf concentrations span within 188 - 231 pmol l^{-1} and 2.2 - 5.6 pmol l^{-1} ranges,
126 respectively. As a consequence, related Zr/Hf values start from 40.8 at 25 m depth, 60.1 at 50 m depth
127 falling close the range of chondritic values (68.9) at 75 m depth. Below 75 m depth Zr and Hf

concentrations fall within narrow ranges: 187.7-206.7 and 2.2-2.6, respectively. Zr/Hf values are almost always above the range of chondritic values, between 92.6 and 78.5 with the maximum found at 200 m depth. So, Zr/Hf ratio remains quite constant along the whole oxic water column and limited changes are observed only in deepest water layers (Fig. 2).

Highest REE concentrations are usually found in shallowest water layers, whereas these values progressively decrease with depth. Below 75 m depth, the overall dissolved REE concentrations range between 326 and 555 pmol $l^{-1}$with a maximum occurring close to 500 m depth. In general, shale-normalised REE patterns show depletion of light REE (LREE) relative to medium and heavy REE (MREE and HREE, respectively), variable extent of Ce anomaly and the progressive growth of normalised concentrations up to Gd. Then, the growth of shale normalised REE concentrations is slighter and the shape of normalised patters are often flat in shape from Ho to Lu. The main difference observed among the features of shale-normalised patters is the extent of Ce anomaly. It does not occur or is few discernible in seawater samples above 75 m depth and progressively along the water column (Fig. 3A). Values of Gd anomaly fall within 1.0 and 1.5 in shallowest waters where a zig-zag behaviour is observed to about 600 m depth. Therefore, Gd anomaly progressively decreases to about 1.2 along the bottom water column where another abrupt growth is observed at close to 3200 m depth. The Y/Ho ratio ranges between 70.5 and 91.4 along the oxic water column. The lowest values are recorder in shallowest water layers between the surface and 75 m depth, whereas the largest is reached in the bottom water between 3000 and 3238 m depth.

3.2 Deep-sea anoxic brines

The related analyses were carried out in deep-sea brines collected in Medee (3078 m depth) and Thetis (3457 m depth) basins where the oxic water column is directly in touch with the underlying anoxic brine. Analyses of brine waters are reported in Tab. 1. In Tyro basin the interface between oxic and anoxic water consists of two layers (upper and lower interface at 3379 and 3380 m depth, respectively) overlying the anoxic brine that was sampled at 3482 m depth.

In Tyro basin Zr and Hf show higher concentrations in lower brine relative to the upper brine layer. The Zr and Hf concentration further decrease from the lower brine to the brine as such. Similar behaviour is shown by Zr/Hf ratio. Zr/Hf ratio is 46.2 in the upper interface. It increases to 72.8 in the lower interface and then decrease and then decreases up to 41.9 in the brine as such. The lowest Zr/Hf value up to 19.5 is observed in the Thetis brine, whereas in Medee brine a Zr/Hf values of 90.5 was measured.

REE concentrations in anoxic deep-sea brines were always higher that in oxic seawater (Fig. 2, Tab. 1). In Tyro basin, the sample from the upper layer of the seawater-brine interface collected at 3379 m depth show a REE concentration close to 3596 pmol kg^{-1}. This value further increases one meter below up to 3731.34 pmol kg^{-1}. Then, the REE concentration falls to 1442.6 pmol kg^{-1} in the brine at 3482 m. In Thetis basin the REE concentration in the brine is 2361.25 pmol kg^{-1} at 3482 m. This value is strongly higher than that found in the lower seawater layer at 3305 m depth that is 2361.25 pmol kg^{-1}. In Medee basin only a brine sample was collected. There, the REE concentration is 2084.89 pmol kg^{-1}.

In Tyro basin Y/Ho values progressively decrease from superchondritic to slight subchondritic values from the upper brine interface to the brine as such. Other brines from Thetis and Medee basins always show Y/Ho values lower than the chondritic signature (Fig. 2).

Shale-normalised REE patterns in these brines are very different in shape relative to oxic seawater. In Tyro brine, $Ce/Ce^* > 1$ values were found from 1 to 1.5, whereas slight negative Ce anomalies were shown both in Thetis and Medee brines (Fig. 3B). The extent of Gd anomaly values ($0.9 \leq Gd/Gd^* \leq 1.3$) is narrower than that recognised in oxic waters with largest value found in Tyro brine (Table 2). The range of Zr/Hf values in brines is wider than that found in oxic waters with higher value found in Tyro brine and lower in Medee.

4. DISCUSSION

4.1 Oxic waters

Figure 4A shows that Zr and Hf concentrations measured along the seawater column below 100 m depth depict a statistically significant linear trend with Zr/Hf = 124 that is intermediate between that characteristic of Upper Crust (71; Rudnick and Gao, 2005) and that the distribution of Zr and Hf concentrations in Eastern Atlantic (156; Godfrey et al., 2009). Recent analyses carried out in Northern Atlantic and Indian Oceans recognised a mean Zr/Hf value close to 402 (Firdaus et al., 2018). This suggests that the Zr-Hf relationship in Eastern Mediterranean seawater can be influenced by interactions between seawater and lithogenic materials delivered to the basin according to different mechanisms. This hypothesis agrees with recent oceanographic data reporting a Zr-Hf relationship characteristic for Marginal seas with Zr/Hf average slope close to 115 for samples collected in the Andaman sea and Gulf of Thailand (Firdaus et al., 2018). On the contrary, shallow waters up to 100 m depth show Zr and Hf concentrations seem falling along a trend with lower slope close to 9. In any case, all the measured Zr/Hf values below 75 m depth in Kryos basin are higher relative to the chondritic values corresponding to 71.4 ± 5.6 (Jochum et al., 1986; 1989) and to the Zr/Hf values of Upper Crust clustered around 71 (Rudnick and Gao, 2005). On the contrary, Zr/Hf values from the shallow waters up to 75 m depth falling on the right side of the trend described by Zr and Hf concentrations measured in other oxic waters in Kryos basin (Fig. 4A).

Taking in account that a significant input of lithogenic products to seawater from continent is represented by the atmospheric fallout (Greaves et al., 1999), a chondritic-to-slight superchondritic signature of Zr/Hf ratio is expected in coastal waters and in the shallowest layers of seawater column (Firdaus et al., 2008; 2018). But the observed dissolved subchondritic Zr/Hf values in shallow seawater layers suggests that the dissolution of a hafnium-enriched solids can occur therein. Thiagarajan and Aeolus-Lee (2004) proposed two suitable mechanisms explaining how Fe-Mn-phosphorous- rich coating of desert particles can be formed (the so-called “Desert varnish”). Several studies evidence that mainly Fe-oxyhydroxides are usually enriched in Hf relative to Zr for the different affinity of Zr and Hf dissolved complexes towards the surface of those solids (Koschinsky and Hein, 2003: 2017; Bau and Koschinsky, 2006; Hein et al., 2013). Since Fe-oxyhydroxides are a

206 main component of the desert varnish (Dorn, 2007; Nash, 2011; Macholdt et al., 2017), the leaching
207 of desert varnish delivered to the Mediterranean surface water from Sahara and Arabian deserts
208 (Guieu et al., 2002; 2005; Censi et al., 2007; Wagener et al., 2008; Goldsmith et al., 2014; Richon et
209 al., 2018; Censi et al., 2015; 2018) can easily determines the observed Hf enrichment of the shallow
210 water layer at Kryos. This agrees with values of Y/Ho ratio that closely behave with Zr/Hf assuming
211 superchondritic (Y/Ho > 52; Nozaki et al., 1997) values characteristic of preferential Ho scavenging
212 onto authigenic suspended particles along the seawater column relative to Y (Nozaki et al., 1997;
213 Censi et al., 2004; 2005; 2007).
214 Zr/Hf and Y/Ho ratios measured in seawater samples above 75 m depth from Kryos basin fall
215 along a trend connecting analyses of desert varnish samples (Thiagarajan and Aeolus-Lee, 2004) and
216 Zr/Hf and Y/Ho values measured in seawater samples below 75 m depth (Fig. 5). This feature
217 contributes to depict a scenario where Zr-Hf and Y-Ho fractionation along the seawater column in
218 Kryos basin is coherent with the dissolution of Fe-rich coating of atmospheric particles and the
219 leaching of these elements in aqueous phase. Here, Zr, Hf, Y and Ho dissolved distribution is a
220 consequence of the equilibrium between the stability of their aqueous complexes and their reactivity
221 towards surfaces of suspended particles along the water column.
222 The lack of negative Ce anomaly and the concurrent LREE enrichment occurring in the
223 shallowest seawater layer (Fig. 3) represent another clue of the influence of dissolution of
224 atmospheric particles in shallow seawater layers. With any probability, the dissolution of lithogenic
225 particles is also responsible of some positive La anomalies observed along the seawater column
226 around 750 m depth (Fig. 6). According to Tachikawa et al. (2004), the dissolving suspended
227 particulate responsible of these positive La anomalies could be originated by the Nile plume.
228 Previous studies postulated that LREE enrichments and lack of positive Ce anomaly in shale-
229 normalised patterns of Mediterranean seawater could be explained in terms of dissolution of particles
230 suspended along the seawater column (Spivack and Wasserburg, 1988; Censi et al., 2007). In order
231 to assess how much this hypothesis can be reasonable, the shale-normalised REE patterns of the

232 shallowest water layers from Kryos basin were compared with that recognised in the shallowest water
233 layer of the sampling site S-470 located in the Strait of Sicily where the atmospheric fallout of desert
234 dust was recognised (Censi et al., 2004). Figure 7 highlight that both these waters show very similar
235 shale-normalised patterns from Nd to Lu, whereas some differences occur as regard of the distribution
236 of LREE. This evidence suggests that this different LREE distribution in shallow waters from Kryos
237 basin and S-470 site can be induced by the dissolution of atmospheric fallout particles since LREE
238 are usually enriched in crustal materials (Haskin and Paster, 1979; Henderson, 1984; Taylor and
239 McLennan, 1995). Accordingly, starting from data reference data the REE concentration of a mixture
240 up to 50 μg kg^{-1} of lithogenic solids formed by desert dust and varnish from Arabian Desert
241 (Goldsmith et al., 2014) was calculated and added to the REE concentration of the shallow water
242 layer from S-470 site. The related shale-normalised pattern was calculated and reported in Fig. 7.
243 Comparing this pattern with that representative of the shallow seawater from Kryos basin, we found
244 that the shallow seawater layer is progressively enriched eastward in LREE easily released by
245 dissolving dust particles coming from Sahara and Arabian deserts (Erel et al., 2013; Ben-Israel et al.,
246 2015).
247
248 *4.2 Deep-sea brines*
249 Zr and Hf values in brines fall within a linear trend with slope 66.5 within the range of
250 chondritic Zr/Hf values (Fig. 4B) indicating that deep-sea brine in Eastern Mediterranean results from
251 dissolution of evaporitic terrains outcropping in seafloor (Cita, 2006 and references therein).
252 Zirconium and Hf concentrations in brines are distributed similarly to measured concentrations
253 of Zr and Hf both in saltworks and Dead Sea (Censi et al., 2017) confirming the hypothesis that the
254 studied brines can be formed by percolation of current seawater through the sediment and dissolution
255 of Messinian evaporites On the other hand, the hypothesis that some Eastern Mediterranean deep-sea
256 brines can also represent relics of evaporated seawater (Vengosh and Starinsky, 1993) cannot be ruled
257 out.

Figure 3B shows almost "flat" shale-normalised REE patterns in studied deep-sea brines collected in Thetis, Medee and Tyro basins where positive Ce anomalies are observed. This requires the possible Ce input from the oxic seawater into the upper interface reflecting the complex transition mechanism between oxic and anoxic waters in Tyro basin Waters (Schijf et al., 1995; Bau et al., 1997). We propose that Ce-enriched oxyhydroxide particles settling through the oxic seawater are dissolved a contact with the oxic-anoxic interface leading to the observed positive Ce anomalies in the upper interface zone of Tyro brine and are responsible for the Ce flux from oxic seawater to the brine. Our data indicate that the positive Ce anomaly disappears in the Tyro brine and this evidence disagrees with data from Bau et a. (1997) where Ce/Ce* =1.7 is shown. The phenomenon is not shown in the deep-sea brine body probably due to the different sampling depth in this study (3482 m) and in Bau et al. (1997) (3400 m).

The extent of Ce and Pr anomaly allows us to illustrate the effects of the delivery of suspended particles from atmospheric fallout to the oxic shallow seawater, their sinking through the oxic water column up to the oxic-anoxic interface (Fig. 6). The classical Ce/Ce* vs Pr/Pr* values in studied waters (redrawn by Bau and Dulski, 1996) shows that:

- both the shallowest water layer from Kryos seawater and the Medee brine are free from either La or Ce anomalies.
- Positive La anomalies are observed in Thetis and Medee brines, in oxic water at 750 and 2500 m depth.
- Positive Ce anomalies are reported in the brines from the lower and upper interfaces in Tyro basin.
- Negative Ce anomalies are observed in other samples from the oxic seawater at Kryos.

The lack of Ce and La anomaly in shallowest Kryos seawater can be determined by the strong contribution of Ce^{3+} released during the dissolution of atmospheric dust particles coupled to the Mn/Fe ratio in Ce-bearing particles forming the desert varnish. Takahashi et al. (2007) show that the Ce concentration in Fe-Mn crusts is determined by their Mn/Fe ratio. As previously discussed, the

284 positive La anomalies recognised at 750 and 2500 m depth can be explained by the dissolution of
285 lithogenic suspended particles delivered through the Nile plume (Tachikawa et al., 2004). Positive
286 Ce anomalies recognised in Tyro brines are determined by the dissolution under reducing conditions
287 in brines of solid CeO_2 enriched in suspended oxic particulate (Saager et al., 1993; Schijf et al., 1995;
288 Bau et al., 1997; Kashiwabara et al., 2018). Negative Ce anomalies through the oxic water are
289 characteristic of the geochemical Ce behaviour in oxic waters.
290
291 5. CONCLUSION
292 The results of this study suggest the occurrence of a relationship between the extent of the Zr/Hf
293 ratio in seawater and nature and origin of the atmospheric dust delivered to the shallow seawater
294 layers where influence the growth of positive La anomalies or the disappearance of negative Ce
295 anomalies typical in marine environment. In Mediterranean, mainly in the eastern basin, the
296 significance of Zr, Hf and REE contribution as atmospheric dust particles is strong, although some
297 evidence of riverine contribution from Nile cannot ruled out.
298 Mainly the Zr/Hf ratio seems suitable to recognise the origin of deep-sea brine filling the anoxic
299 trenches in Thetis, Medee and Tyro basins as due to the dissolution of evaporites from Messinian
300 sequences outcropping in the seafloor. This process determines Zr/Hf values close to the signature
301 characteristic of crustal rocks of slight lower, probably as consequence of the larger Hf affinity
302 towards the surface of salt minerals relative to Zr. In general, Eastern Mediterranean seawater shows
303 larger dissolved Zr, Hf and REE concentrations than Atlantic. Taking in account that Eastern
304 Mediterranean is the basin where the outflow current to Atlantic Ocean is forming, the overall
305 Mediterranean Sea represents a source of the studied trace elements for the Atlantic.

307 Acknowledgements

308 We are indebted to Dr. M. Yakimov and his team for facilities offered to the authors during the
309 Mamba 2010 oceanographic cruise. This paper reports scientific results belonging to the PhD project
310 of Maria Raso. This research was partially funded by the contract CORI 2012 and 2017 (University
311 of Palermo).

313 REFERENCES

314 Alibo, D.S., Nozaki, Y., 1999. Rare earth elements in seawater: Particle association, shale-
315 normalization, and Ce oxidation. Geochim Cosmochim Ac 63, 363-372.
316 Bau, M., Dulski, P., 1996. Distribution of yttrium and rare-earth elements in the Penge and Kuruman
317 iron-formations, Transvaal Supergroup, South Africa. Precambrian Res 79, 37-55.
318 Bau, M.; Moller, P.; Dulski, P., 1997. Yttrium and lanthanides in eastern Mediterranean seawater and
319 their fractionation during redox-cycling. Marine Chemistry 56, (1-2), 123-131.
320 Camerlenghi, A., 1990. Anoxic Basins of the Eastern Mediterranean - Geological Framework. Marine
321 Chemistry 31, (1-3), 1-19.
322 Censi, P., Cangemi, M., Brusca, L., Madonia, P., Saiano, F., Zuddas, P., 2015. The behavior of rare-
323 earth elements, Zr and Hf during biologically-mediated deposition of silica-stromatolites and
324 carbonate-rich microbial mats. Gondwana Research 27, 209-215.
325 Censi, P., Inguaggiato, C., Chiavetta, S., Schembri, C., Sposito, F., Censi, V., Zuddas, P., 2017. The
326 behaviour of zirconium, hafnium and rare earth elements during the crystallisation of halite and
327 other salt minerals. Chem Geol 453, 80-91.
328 Censi, P., Sposito, F., Inguaggiato, C., Zuddas, P., Inguaggiato, S., Venturi, M., 2018. Zr, Hf and
329 REE distribution in river water under different ionic strength conditions. Science of the Total
330 Environment 645, 837-853.
331 Censi, P., Spoto, S.E., Nardone, G., Saiano, F., Punturo, R., Di Geronimo, S.I., Mazzola, S., Bonanno,
332 A., Patti, B., Sprovieri, M., Ottonello, D., 2005. Rare-earth elements and yttrium distributions
333 in mangrove coastal water systems: The western Gulf of Thailand. Chemistry and Ecology 21,
334 255-277.
335 Censi, P.; Mazzola, S.; Sprovieri, M.; Bonanno, A.; Patti, B.; Punturo, R.; Spoto, S. E.; Saiano, F.;
336 Alonzo, G., 2004. Rare earth elements distribution in seawater and suspended particulate of the
337 Central Mediterranean Sea. Chemistry and Ecology 20, (5), 323-343.

338 Censi, P.; Randazzo, L. A.; Zuddas, P.; Saiano, F.; Aricò, P.; Andò S., 2010. Trace element behaviour
339 in seawater during Etna's pyroclastic activity in 2001: Concurrent effects of nutrients and
340 formation of alteration minerals. Journal of Volcanology and Geothermal Research 193, (1-2),
341 106-116.
342 Censi, P.; Sprovieri, M.; Larocca, D.; Aricò, P.; Saiano, F.; Mazzola, S.; Ferla, P., 2007. Alteration
343 effects of volcanic ash in seawater: Anomalous Y/Ho ratios in coastal waters of the Central
344 Mediterranean Sea. Geochimica et Cosmochimica Acta 71, (22), 5405-5422.
345 Cita, M.B., 2006. Exhumation of Messinian evaporites in the deep-sea and creation of deep anoxic
346 brine-filled collapsed basins. Sedimentary Geology 188-189, 357-378.
347 Dorn, R.I., 2007. Baking black opal in the desert sun: The importance of silica in desert varnish:
348 Comment. Geology 35, e122-e123.
349 Firdaus, M.L., Darti, P., Alwi, W., Swistoro, E., Sundaryono, A., Ruyani, A., 2015. Trace metals
350 geochemistry of Bengkulu river and estuary, AIP Conference Proceedings.
351 Firdaus, M.L., Mashio, A.S., Obata, H., McAlister, J.A., Orians, K.J., 2018. Distribution of zirconium,
352 hafnium, niobium and tantalum in the North Atlantic Ocean, northeastern Indian Ocean and its
353 adjacent seas. Deep-Sea Research Part I: Oceanographic Research Papers 140, 128-135.
354 Firdaus, M.L., Minami, T., Norisuye, K., Sohrin, Y., 2011. Strong elemental fractionation of Zr-Hf
355 and Nb-Ta across the Pacific Ocean. Nature Geoscience 4, 227-230.
356 Firdaus, M.L., Norisuye, K., Sato, T., Urushihara, S., Nakagawa, Y., Umetani, S., Sohrin, Y., 2007.
357 Preconcentration of Zr, Hf, Nb, Ta and W in seawater using solid-phase extraction on TSK-8-
358 hydroxyquinoline resin and determination by inductively coupled plasma-mass spectrometry.
359 Analytica Chimica Acta 583, 296-302.
360 Godfrey, L. V.; White, W. M.; Salters, V. J. M., 1996. Dissolved zirconium and hafnium distributions
361 across a shelf break in the North-Eastern Atlantic Ocean. Geochimica et Cosmochimica Acta
362 60, (21), 3995-4006.

363 Godfrey, L.V., Field, M.P., Sherrell, R.M., 2008. Estuarine distributions of Zr, Hf, and Ag in the
364 Hudson River and the implications for their continental and anthropogenic sources to seawater.
365 Geochemistry, Geophysics, Geosystems 9.
366 Godfrey, L.V., Zimmermann, B., Lee, D.C., King, R.L., Vervoort, J.D., Sherrell, R.M., Halliday,
367 A.N., 2009. Hafnium and neodymium isotope variations in NE Atlantic seawater.
368 Geochemistry, Geophysics, Geosystems 10.
369 Goldsmith, Y., Stein, M., Enzel, Y., 2014. From dust to varnish: Geochemical constraints on rock
370 varnish formation in the Negev Desert, Israel. Geochim Cosmochim Ac 126, 97-111.
371 Greaves, M. J.; Elderfield, H.; Sholkovitz, E. R., 1999. Aeolian sources of rare earth elements to the
372 Western Pacific Ocean. Marine Chemistry 68, (1-2), 31-38.
373 Greaves, M. J.; Rudnicki, M.; Elderfield, H., 1991. Rare earth elements in the Mediterranean Sea and
374 mixing in the Mediterranean outflow. Earth and Planetary Science Letters 103, (1-4), 169-181.
375 Greaves, M. J.; Statham, P. J.; Elderfield, H., 1994. Rare earth element mobilization from marine
376 atmospheric dust into seawater. Marine Chemistry 46, (3), 255-260.
377 Guieu, C., Bonnet, S., Wagener, T., Loÿe-Pilot, M.D., 2005. Biomass burning as a source of dissolved
378 iron to the open ocean? Geophysical Research Letters 32, 1-5.
379 Guieu, C., Bozec, Y., Blain, S., Ridame, C., Sarthou, G., Leblond, N., 2002. Impact of high Saharan
380 dust inputs on dissolved iron concentrations in the Mediterranean Sea. Geophysical Research
381 Letters 29, 17-11.
382 Guieu, C., Shevchenko, V.P., 2016. Dust in the ocean, Encyclopedia of Earth Sciences Series, pp.
383 203-208.
384 Haskin, L.A., Paster, T.P., 1979. Chapter 21 Geochemistry and mineralogy of the rare earths,
385 Handbook on the Physics and Chemistry of Rare Earths, pp. 1-80.
386 Hein, J.R., Mizell, K., Koschinsky, A., Conrad, T.A., 2013. Deep-ocean mineral deposits as a source
387 of critical metals for high- and green-technology applications: Comparison with land-based
388 resources. Ore Geology Reviews 51, 1-14.

389 Henderson, P., 1984. General geochemical properties and abundance of the REE. REE Geochemistry,
390 253-281.
391 Hsu, K.J.; Montadert, L. et al (Editors), 1978. Initial Reports DSDP, 42, Part 1. U.S. Government
392 Printing Office, Washington, D.C., 1249 pp.
393 Jochum, K.P., McDonough, W.F., Palme, H., Spettel, B., 1989. Compositional constraints on the
394 continental lithospheric mantle from trace elements in spinel peridotite xenoliths. Nature 340,
395 548-550.
396 Jochum, K.P., Seufert, H.M., Spettel, B., Palme, H., 1986. The solar-system abundances of Nb, Ta,
397 and Y, and the relative abundances of refractory lithophile elements in differentiated planetary
398 bodies. Geochim Cosmochim Ac 50, 1173-1183.
399 Kashiwabara, T., Toda, R., Nakamura, K., Yasukawa, K., Fujinaga, K., Kubo, S., Nozaki, T.,
400 Takahashi, Y., Suzuki, K., Kato, Y., 2018. Synchrotron X-ray spectroscopic perspective on the
401 formation mechanism of REY-rich muds in the Pacific Ocean. Geochim Cosmochim Ac 240,
402 274-292.
403 Koschinsky, A., Hein, J.R., 2003. Uptake of elements from seawater by ferromanganese crusts: Solid-
404 phase associations and seawater speciation. Marine Geology 198, 331-351.
405 Koschinsky, A., Hein, J.R., 2017. Marine ferromanganese encrustations: Archives of changing
406 oceans. Elements 13, 177-182.
407 Lutfi Firdaus, M., Norisuye, K., Nakagawa, Y., Nakatsuka, S., Sohrin, Y., 2008. Dissolved and labile
408 particulate Zr, Hf, Nb, Ta, Mo and W in the western North Pacific Ocean. Journal of
409 Oceanography 64, 247-257.
410 Macholdt, D.S., Jochum, K.P., Pöhlker, C., Arangio, A., Förster, J.D., Stoll, B., Weis, U., Weber, B.,
411 Müller, M., Kappl, M., Shiraiwa, M., Kilcoyne, A.L.D., Weigand, M., Scholz, D., Haug, G.H.,
412 Al-Amri, A., Andreae, M.O., 2017. Characterization and differentiation of rock varnish types
413 from different environments by microanalytical techniques. Chemical Geology 459, 91-118.

MEDRIFF Consortium, 1995. Three brine lakes discovered in the seafloor of the eastern Mediterranean. *EOS Trans AGU*, 76: 313.

Möller, P., Rosenthal, E., Geyer, S., Guttman, J., Dulski, P., Rybakov, M., Zilberbrand, M., Jahnke, C., Flexer, A., 2007. Hydrochemical processes in the lower Jordan valley and in the Dead Sea area. Chem Geol 239, 27-49.

Nozaki, Y., Zhang, J., Amakawa, H., 1997. The fractionation between Y and Ho in the marine environment. Earth Planet Sc Lett 148, 329-340.

Raso M., Saiano F., Censi P., 2012. A new method for simultaneous determinations of REE, Zr and Hf in natural waters. Talanta 116, 1085-1090.

Richon, C., Dutay, J.C., Dulac, F., Wang, R., Balkanski, Y., 2018. Modeling the biogeochemical impact of atmospheric phosphate deposition from desert dust and combustion sources to the Mediterranean Sea. Biogeosciences 15, 2499-2524.

Rickli, J., Gutjahr, M., Vance, D., Fischer-Gödde, M., Hillenbrand, C.D., Kuhn, G., 2014. Neodymium and hafnium boundary contributions to seawater along the West Antarctic continental margin. Earth and Planetary Science Letters 394, 99-110.

Rudnick, R.L., Gao, S., 2003. Composition of the Continental Crust, Treatise on Geochemistry, pp. 1-64.

Ryan, W.F.B.; Hsu, K.J. et al., 1993. Initial Reports DSDP, 13, Part 1. U.S. Government Printing Office, Washington, DC, 514 pp.

Saager, P.M., Schijf, J., de-Baar, H.J.W., 1993. Trace-Metal Distributions in Seawater and Anoxic Brines in the Eastern Mediterranean-Sea. Geochim Cosmochim Ac 57, 1419-1432.

Schijf, J., De Baar, H. J. W., Millero, F. J., 1995. Vertical Distributions and Speciation of Dissolved Rare-Earth Elements in the Anoxic Brines of Bannock Basin, Eastern Mediterranean-Sea. Geochimica et Cosmochimica Acta 59, (16), 3285-3299.

438 Schmidt, K., Bau, M., Hein, J.R., Koschinsky, A., 2014. Fractionation of the geochemical twins Zr-
439 Hf and Nb-Ta during scavenging from seawater by hydrogenetic ferromanganese crusts.
440 Geochim Cosmochim Ac 140, 468-487.
441 Spivack, A.J., Wasserburg, G.J., 1988. Neodymium isotopic composition of the Mediterranean
442 outflow and the eastern North Atlantic. Geochim Cosmochim Acta 52, 2767-2773.
443 Tachikawa, K., Jeandel, C., Dupré, B., 1997. Distribution of rare earth elements and neodymium
444 isotopes in settling particulate material of the tropical Atlantic Ocean (EUMELI site). Deep-
445 Sea Research Part I: Oceanographic Research Papers 44, 1769-1792.
446 Tachikawa, K., Jeandel, C., Vangriesheim, A., Dupré, B., 1999. Distribution of rare earth elements
447 and neodymium isotopes in suspended particles of the tropical Atlantic Ocean (EUMELI site).
448 Deep-Sea Research Part I: Oceanographic Research Papers 46, 733-755.
449 Tachikawa, K., Roy-Barman, M., Michard, A., Thouron, D., Yeghicheyan, D., Jeandel, C., 2004.
450 Neodymium isotopes in the Mediterranean Sea: Comparison between seawater and sediment
451 signals. Geochim Cosmochim Ac 68, 3095-3106.
452 Takahashi, Y., Hirata, T., Shimizu, H., Ozaki, T., Fortin, D., 2007. A rare earth element signature of
453 bacteria in natural waters? Chemical Geology 244, 569-583.
454 Taylor, S.R., McLennan, S.M., 1995. The geochemical evolution of the continental crust. Reviews
455 of Geophysics 33, 241-265.
456 Thiagarajan, N., Aeolus-Lee, C.T., 2004. Trace-element evidence for the origin of desert varnish by
457 direct aqueous atmospheric deposition. Earth Planet Sc Lett 224, 131-141.
458 Vengosh, A., Starinsky, A., 1993. Relics of Evaporated Sea-Water in Deep Basins of the Eastern
459 Mediterranean. Marine Geology 115, 15-19.
460 Wagener, T., Pulido-Villena, E., Guieu, C., 2008. Dust iron dissolution in seawater: Results from a
461 one-year time-series in the Mediterranean Sea. Geophysical Research Letters 35. Alibo, D. S.;
462 Nozaki, Y., 1999. Rare earth elements in seawater: Particle association, shale-normalization,
463 and Ce oxidation. Geochimica et Cosmochimica Acta 63, (3-4), 363-372.

TABLE CAPTIONS

Table 1 – Trace element concentrations, selected ratios and anomalies measured in studied samples collected at different sampling depth from studied sites.

FIGURE CAPTIONS

Figure 1 – Schematic sketch map of studied sites.

Figure 2 – Distribution of the overall REE concentration, values of Zr/Hf and Y/Ho ratios and extent of Gd and Ce anomaly values along the studied oxic seawater column in Kryos basin (A), through the interface between seawater and underlying brine in Tyro (B) and Thetis basins (C), in the deep-sea brine in Medee basin (D).

Figure 3 – Shale-normalised REE patterns calculated relative to Post Archean Australian Shale (PAAS) (Taylor and McLennan, 1995). A: Oxic seawater from Kryos and Thetis basins. B: Brines from Tyro, Thetis and Medee basins. Red patterns represent waters collected above 75 m depth.

Figure 4 – A: Zr vs. Hf concentrations in seawater samples above 100 m depth (red dots) and seawater samples below 100 m depth (black dots) compared with representative data collected in Northern, Eastern Atlantic, Indian Ocean and related marginal basins (Andaman Sea and Gulf of Thailand) by Firdaus et al. (2018). B: Zr vs. Hf concentrations in brine samples analysed in this study (red dots) compared with analyses carried out in saltworks and Dead Sea brines (blue full squares) by Censi et al. (2017).

Figure 5 – Zr/Hf vs. Y/Ho values measured in seawater samples above 100 m depth (red dots) and in seawater samples below 100 m depth (black dots) compared with values calculated from desert varnish samples reported in Thiagarajan and Aeolus-Lee (2004).

Figure 6 – Ce/Ce* vs. Pr/Pr* values depicted for discriminating samples showing positive or negative Ce and La anomalies (from Bau and Dulski, 1996).

Figure 7 - Shale-normalised REE pattern relative to the composition of the shallow seawater at 25 m in Kryos basin compared with the composition of the shallow seawater in the S-470 station from the Strait of Sicily (Censi et al., 2004).

- (S-470/10) analysed concentrations
- (DV-10) analysed concentrations added with 10 μg kg^{-1} of desert varnish obtained by Goldsmith et al. (2014);
- (DV-30) analysed concentrations added with 30 μg kg^{-1} of desert varnish obtained by Goldsmith et al. (2014).
- (DV-40) analysed concentrations added with 30 μg kg^{-1} of desert varnish obtained by Goldsmith et al. (2014).

500 Table 1 - Trace element concentrations, selected ratios and anomalies measured in studied samples collected at different sampling depth from studied sites.

501

	depth m	Y	La	Ce	Pr	Nd	Sm	Eu	Gd	Tb	Dy	Ho	Er	Tm	Yb	Lu	Hf	Zr	REE	Y/Ho	Zr/Hf	Ce/Ce*	Gd/Gd*
										pmol Kg^{-1}												
Kryos	25	232.0	78.4	130.5	11.0	36.4	10.4	2.6	13.3	2.3	14.2	3.3	9.6	1.4	8.7	1.3	5.6	228.6	555.2	70.5	40.8	1.0	1.0
Kryos	50	219.3	46.5	42.3	8.8	29.3	9.1	2.1	11.0	1.7	10.8	2.8	8.4	1.2	7.6	1.1	3.3	200.5	402.0	79.5	60.1	0.5	1.2
Kryos	75	221.0	75.8	73.2	10.0	33.3	9.3	1.8	11.8	1.5	10.6	2.6	8.2	1.2	7.3	1.0	3.0	209.6	468.7	84.9	68.9	0.6	1.5
Kryos	100	239.0	42.4	33.4	8.4	28.7	8.5	2.0	10.8	1.6	11.3	2.7	9.0	1.3	8.0	1.2	2.6	200.6	408.3	87.3	78.5	0.4	1.3
Kryos	200	233.8	44.7	31.6	9.1	29.7	8.8	1.8	11.9	1.6	11.4	2.7	9.0	1.2	7.9	1.2	2.5	231.4	406.2	87.4	93.5	0.4	1.5
Kryos	300	229.4	42.5	30.0	9.1	28.3	8.5	1.8	10.7	1.5	11.0	2.7	8.7	1.3	8.2	1.2	2.4	195.7	394.8	85.4	80.1	0.4	1.4
Kryos	500	244.0	41.0	24.2	7.8	27.5	7.9	1.9	10.5	1.6	11.8	2.8	9.3	1.3	8.4	1.2	2.5	208.3	401.3	87.1	82.9	0.3	1.3
Kryos	750	223.9	94.4	91.0	10.6	45.1	9.1	1.8	11.9	1.4	10.7	2.6	8.9	1.2	7.9	1.2	2.5	207.0	521.8	85.1	84.0	0.6	1.7
Kryos	1500	205.1	28.8	18.9	6.0	20.3	6.1	1.7	8.0	1.4	10.0	2.4	8.0	1.1	7.3	1.1	2.3	187.7	326.3	87.0	81.5	0.3	1.1
Kryos	2500	215.4	48.5	38.4	5.4	30.1	6.1	1.7	9.7	1.4	10.2	2.5	8.2	1.2	7.6	1.2	2.5	200.3	387.5	85.9	80.3	0.5	1.4
Kryos	3000	214.0	35.1	25.1	6.5	24.3	6.1	1.6	9.1	1.4	10.1	2.3	8.3	1.1	7.4	1.1	2.2	193.9	353.4	91.4	86.4	0.4	1.3
Kryos	3190	205.5	45.6	35.0	6.9	29.7	6.4	1.6	12.0	1.3	9.5	2.3	7.6	1.1	7.3	1.1	2.3	202.3	372.9	89.2	86.7	0.4	1.9
Kryos	3238	213.1	41.9	28.1	6.5	24.7	6.3	1.6	8.8	1.4	9.9	2.5	8.0	1.1	7.2	1.1	2.3	197.8	362.3	86.1	85.0	0.4	1.2
Tyro upper interface	3379	1349.2	480.9	1065.1	70.0	255.0	64.7	18.0	75.4	14.3	72.9	19.3	49.6	8.9	43.7	9.3	33.6	1556.8	3596.4	69.9	46.4	1.3	0.9
Tyro lower interface	3380	992.2	550.4	1387.1	80.0	332.9	68.7	16.3	88.7	12.0	71.2	17.7	52.2	7.4	45.7	8.7	39.5	2874.2	3731.3	55.9	72.8	1.5	1.3
Tyro brine	3482	319.7	285.1	479.1	40.9	135.7	31.9	10.5	37.5	6.6	32.7	8.8	22.1	4.3	22.1	5.3	12.5	522.2	1442.6	36.2	41.9	1.0	1.0
Thetis SW	3305	216.7	48.8	29.7	7.4	27.5	7.5	1.9	9.2	1.6	10.3	2.6	8.4	1.2	7.8	1.2	2.6	249.1	381.8	83.3	97.6	0.4	1.1
Tethis brine	3457	815.4	581.3	476.6	44.9	149.7	47.7	12.0	58.0	9.5	58.7	13.7	40.5	6.1	39.6	7.6	6.2	121.7	2361.2	59.5	19.5	0.6	1.1
Medee brine	3079	608.6	395.7	566.0	54.4	176.2	53.1	13.5	60.3	10.0	44.7	12.5	34.7	6.5	41.8	6.9	10.5	954.4	2084.9	48.8	90.5	0.9	1.0

502

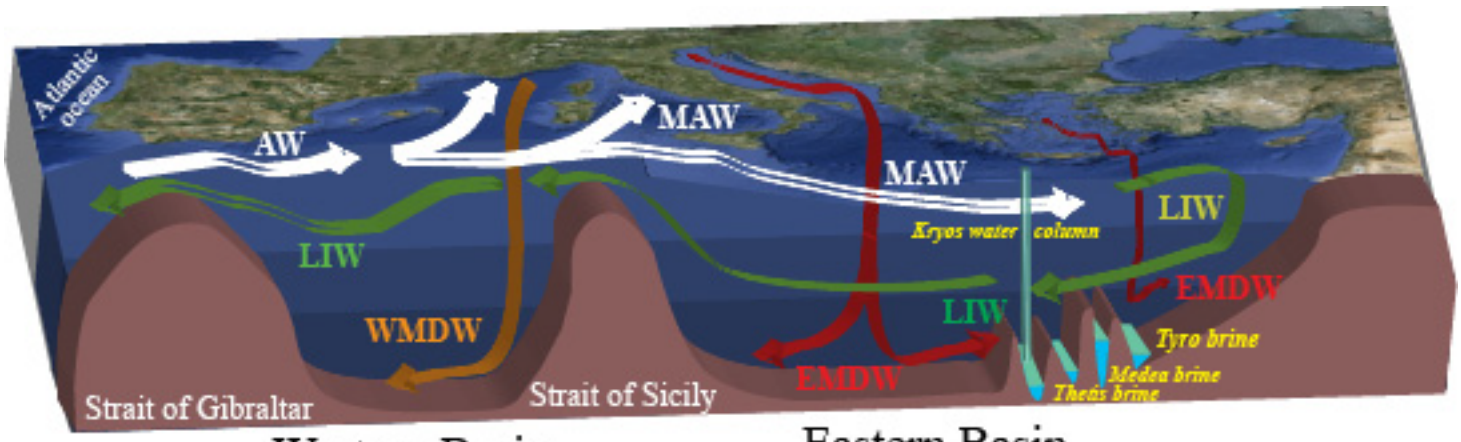
Atlantic ocean
AW
MAW
MAW
LIW
Kryos water column
LIW
EMDW
LIW
WMDW
Tyro brine
Medea brine
Thetis brine
EMDW
Strait of Gibraltar
Strait of Sicily
Western Basin
Eastern Basin

Figure 1

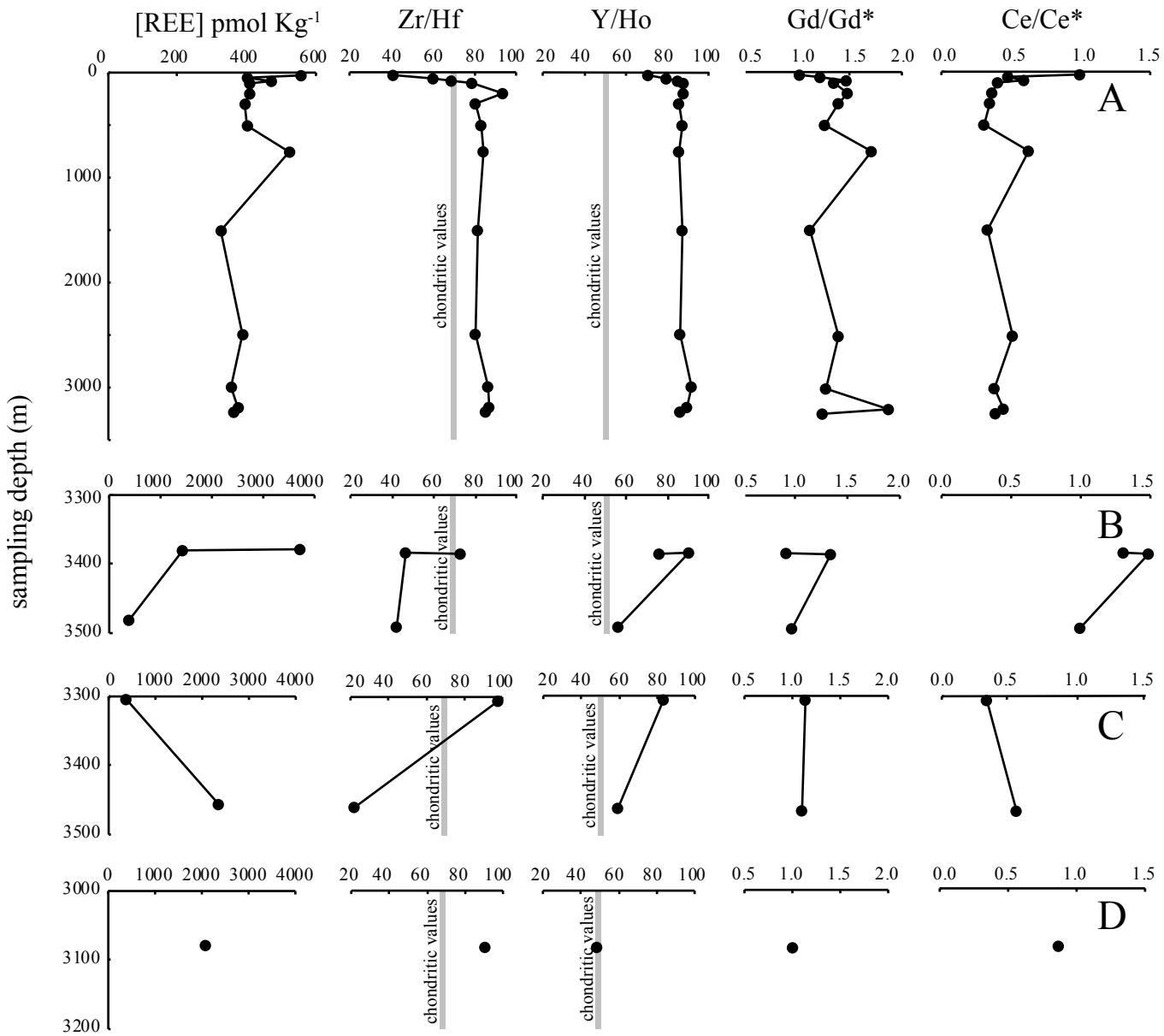
[REE] pmol Kg-1
Zr/Hf
Y/Ho
Gd/Gd*
Ce/Ce*
sampling depth (m)
chondritic values
A
B
C
D

Fig. 2

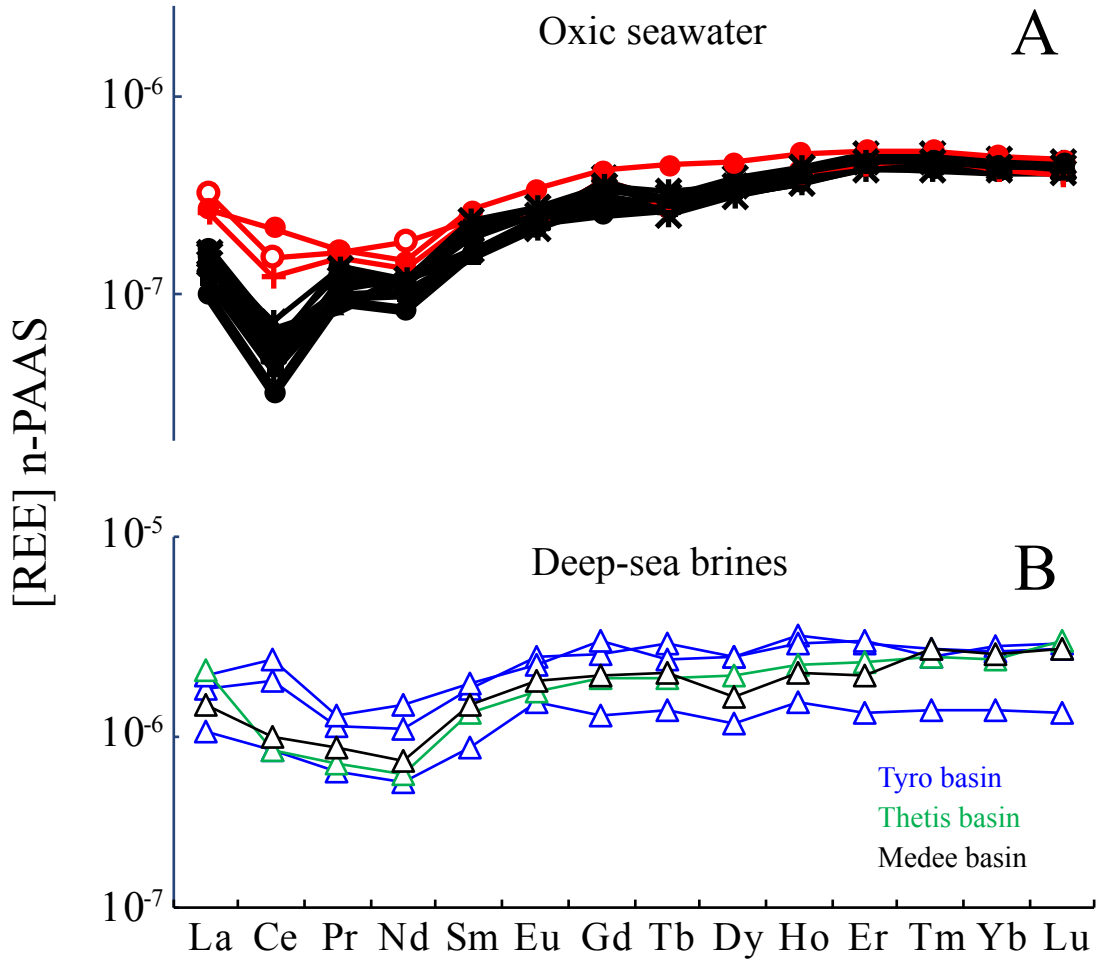
Oxic seawater
A
10-6
10-7
[REE] n-PAAS
10-5
Deep-sea brines
B
10-6
10-7
Tyro basin
Thetis basin
Medee basin
La Ce Pr Nd Sm Eu Gd Tb Dy Ho Er Tm Yb Lu

Fig. 3

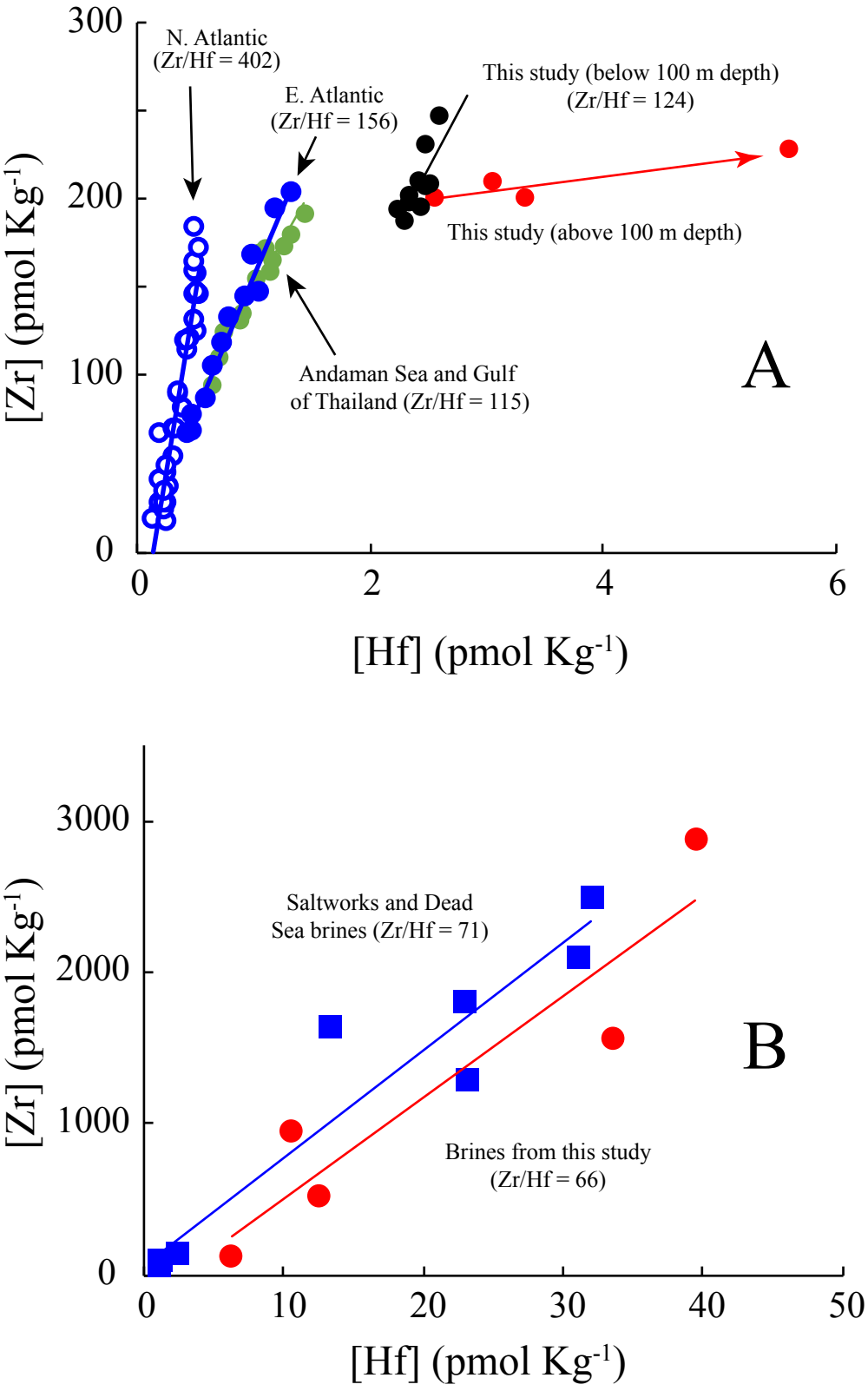
300
200
100
0
[Zr] (pmol Kg-1)
N. Atlantic
(Zr/Hf = 402)
E. Atlantic
(Zr/Hf = 156)
This study (below 100 m depth)
(Zr/Hf = 124)
This study (above 100 m depth)
Andaman Sea and Gulf
of Thailand (Zr/Hf = 115)
A
0
2
4
6
[Hf] (pmol Kg-1)
3000
2000
1000
0
[Zr] (pmol Kg-1)
Saltworks and Dead
Sea brines (Zr/Hf = 71)
B
Brines from this study
(Zr/Hf = 66)
0
10
20
30
40
50
[Hf] (pmol Kg-1)

Fig. 4

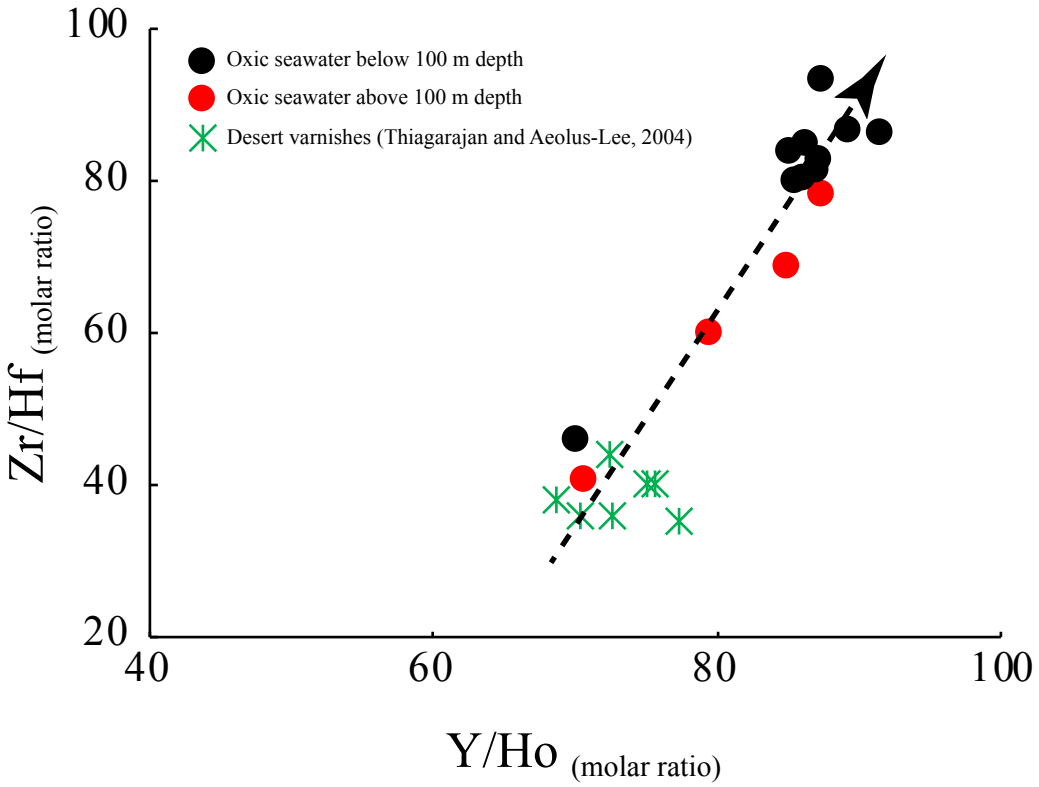
Oxic seawater below 100 m depth
Oxic seawater above 100 m depth
Desert varnishes (Thiagarajan and Aeolus-Lee, 2004)
Zr/Hf (molar ratio)
Y/Ho (molar ratio)
100
80
60
40
20
40
60
80
100

Fig. 5

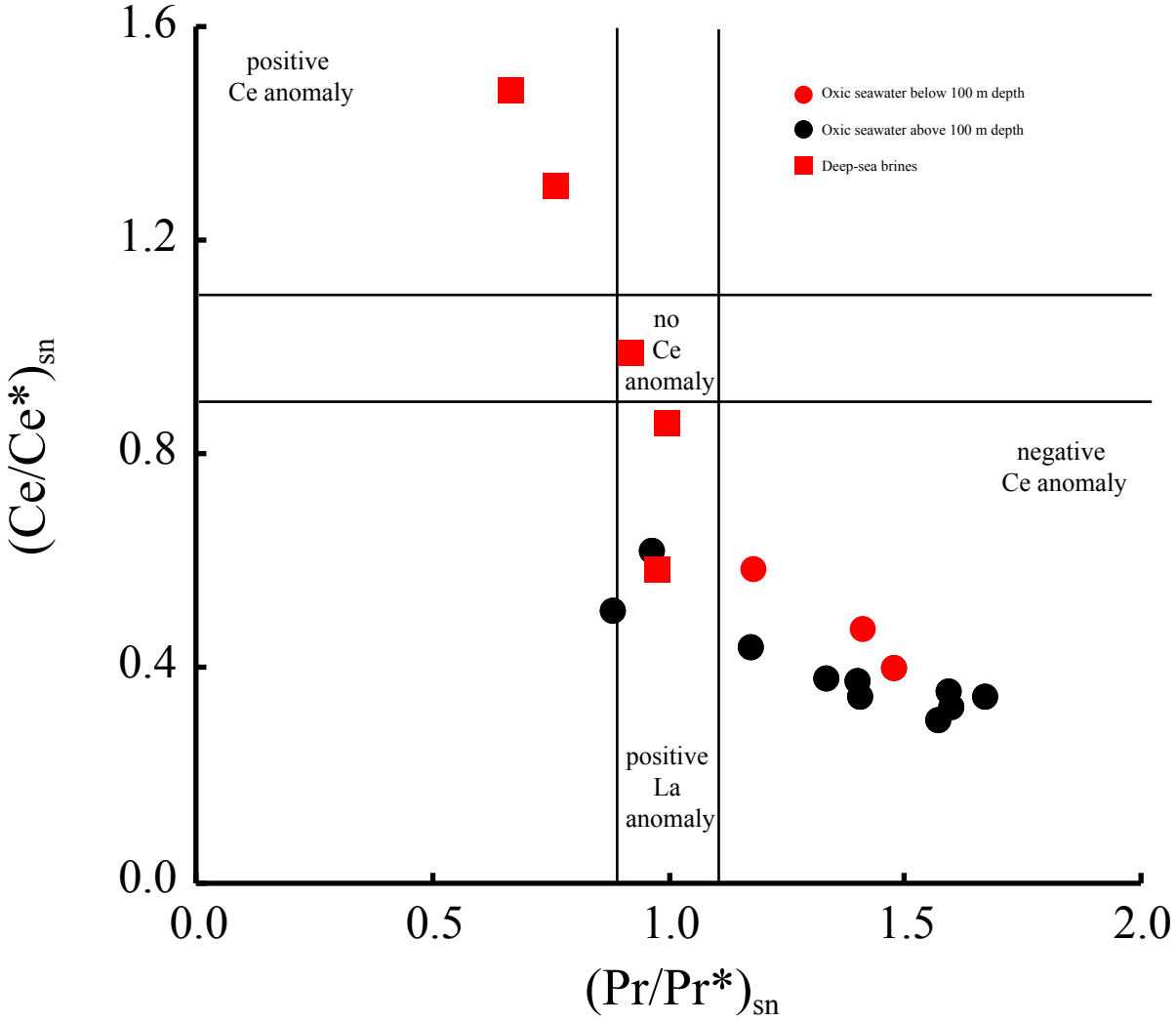
1.6
1.2
0.8
0.4
0.0
0.0
0.5
1.0
1.5
2.0
(Ce/Ce*)sn
(Pr/Pr*)sn
positive
Ce anomaly
no
Ce
anomaly
negative
Ce anomaly
positive
La
anomaly
Oxic seawater below 100 m depth
Oxic seawater above 100 m depth
Deep-sea brines

Fig. 6

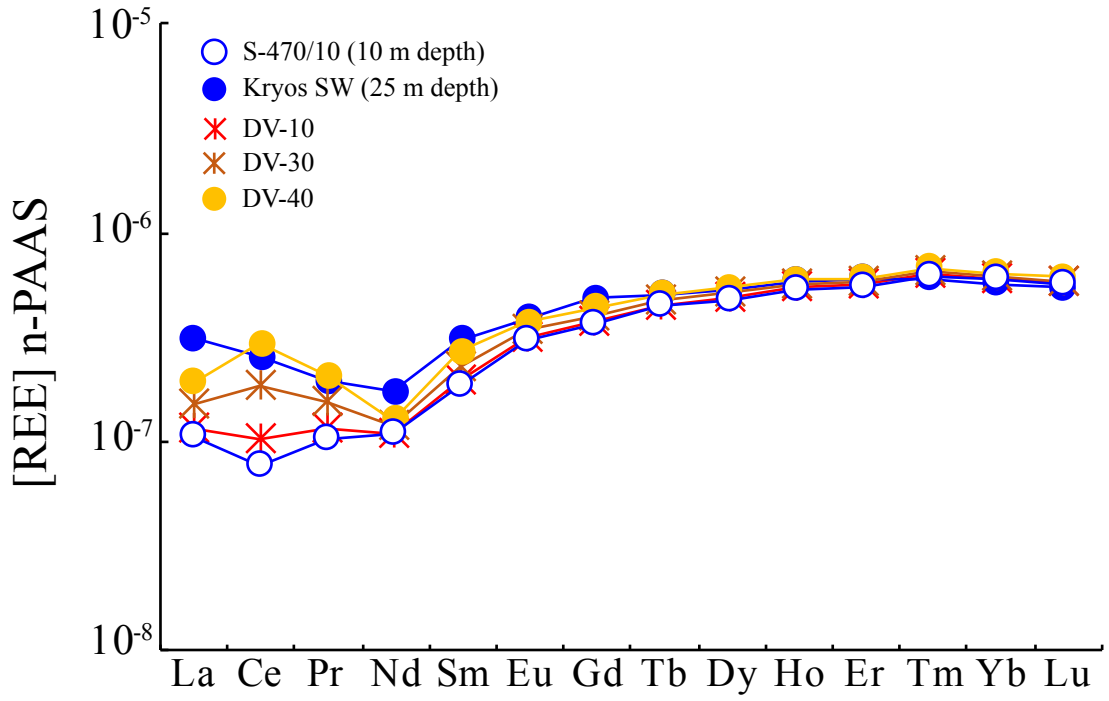
S-470/10 (10 m depth)
Kryos SW (25 m depth)
DV-10
DV-30
DV-40
[REE] n-PAAS
10-5
10-6
10-7
10-8
La Ce Pr Nd Sm Eu Gd Tb Dy Ho Er Tm Yb Lu

Fig. 7